JOURNAL OF COMPUTATIONAL PHYSICS **143,** 403–425 (1998)
ARTICLE NO. CP985943

A Reduced-Order Method for Simulation and Control of Fluid Flows[1]

K. Ito and S. S. Ravindran[2]

Center for Research in Scientific Computation, Department of Mathematics, North Carolina State University, Raleigh, North Carolina 27695-8205
E-mail: kito@eos.ncsu.edu, ravi@eos.ncsu.edu

Received September 18, 1996; revised December 9, 1997

This article presents a reduced-order modeling approach for simulation and control of viscous incompressible flows. The reduced-order models suitable for control and which capture the essential physics are developed using the reduced-basis method. The so-called Lagrange approach is used to define reduced bases and the basis functions in this approach are obtained from the numerical solutions. The feasibility of this method for flow control is demonstrated on boundary control problems in closed cavity and in wall-bounded channel flows. Control action is effected through boundary surface movement on a part of the solid wall. Our formulation of the reduced-order method applied to flow control problems leads to a constrained minimization problem and is solved by applying Newton-like methods to the necessary conditions of optimality. Through our computational experiments we demonstrate the feasibility and applicability of the reduced-order method for simulation and control of fluid flows.

Key Words: reduced-basis method; reduced-order modeling; Navier–Stokes equations; finite element; optimal control.

CONTENTS

[1] Supported in part by the Air Force Office of Scientific Research under Grants AFOSR F49620-95-1-0437 and AFOSR F49620-95-1-0447.

[2] Currently at Flow Modeling and Control Branch, NASA Langley Research Center, Hampton, VA 23681. (ravi@fmd00.larc.nasa.gov)

0021-9991/98 $25.00

1. INTRODUCTION

Control problems that involve partial differential equations as state equations are formidable problems to solve in real time. One such situation arises in control of fluid dynamical systems in which the state equations are the Navier–Stokes equations; see, e.g. [2–4, 6–8, 16] for works on fluid flow control.

In this article, we discuss a reduction-type method which may help to overcome this difficulty. This method, called the reduced-basis method, uses functions as basis functions which are closely related to the problem that is being solved. This is in contrast to the traditional numerical methods such as the finite difference method which uses grid functions as basis functions or the finite elements method which uses piecewise polynomials for this purpose.

We will use the so-called Lagrange approach to generate basis functions in our simulation and control discussions. In the Lagrange approach one uses solutions of the problem at various parameter values as basis functions. We will also briefly discuss another approach called the Hermite approach which uses solutions and their first derivatives at various parameter values as basis functions. Finally, we mention the Taylor approach in which one uses solutions at a point, along with their derivatives as basis functions.

The reduced basis has been applied to structural mechanics problems with considerable success, see [1, 11–14]. Its use for high Reynolds number fluid flow calculation has been shown; see [15].

Our goal here is first to test and validate the reduced-basis method for fluid flow simulations. Then we use the resulting reduced-order model for control problems in fluid flows. We will investigate both steady and unsteady flows and demonstrate the feasibility of the reduced-order model for simulation and control of fluid flows by performing computations on cavity, backward-facing-step channel flow, and forward-facing-step channel flow. An optimal control problem is first formulated and then this problem is approximated by the reduced-basis method. The resulting reduced-order control problem is solved for the control. As a consequence the computed control provides a suboptimal control to the original optimal control problem. Our numerical results indicate that the control computed this way can indeed give very good performance when applied to the original optimal control problem.

1.1 *Reduced basis subspaces.* In order to illustrate the reduced-basis method, we assume for ease in exposition that we are dealing with nonlinear dynamics about stable equilibrium points. Consider the parameterized stationary problem

$$E(y, \mu) = 0 \quad \text{for } \mu \in \mathbb{R}, y \in X, \tag{1.1}$$

where μ represents some physical parameter, for example, a Reynolds number or viscosity, about which we choose to interpolate to obtain a reduced-finite-dimensional set of basis elements. In standard finite element approximations, one approximates X with a piecewise polynomial space. However, the choices for the reduced basis method are different.

The Lagrange subspace. In this case, the basis elements are solutions of the nonlinear problem under study at various parameter values μ_j. The reduced subspace is given by

$$X_R = \text{span}\{y^j \mid y^j = y(\mu_j),\ j = 1, \ldots, M\}.$$

This kind of subspace was used to study structural problems in [1]. A possible advantage in this choice is that updating the basis elements can be done one basis vector at a time instead of generating the whole space.

The Hermite subspace. In this case the basis elements are solutions and their first derivatives at various parameter values μ_j. The reduced subspace is given by

$$X_R = \text{span}\left\{y^j = y(\mu_j) \text{ and } \left.\frac{\partial y}{\partial \mu}\right|_{\mu=\mu_j},\ j = 1, \ldots, \tilde{M}\right\}.$$

The Taylor subspace. In this case, one assumes at some value of μ, say μ^*, the solution is known and it has M derivatives. Then the reduced basis subspace X_R is defined as

$$X_R = \text{span}\left\{y_j \mid y_j = \left.\frac{\partial^j y}{\partial \mu^j}\right|_{\mu=\mu^*},\ j = 0, \ldots, M\right\},$$

where y^j is obtained from successive differentiation of (1.1). This choice has been extensively used in the literature; see e.g. [11, 12] for structural analysis problems and [15] for high Reynolds number steady state fluid flow calculations.

In our calculations, we only employ Lagrange and Hermite approaches due to the following reasons. The equation which is solved to find y_j in the Taylor approach can be ill-posed and one cannot continue to use the same basis elements generated at fixed parameter μ^* to compute solutions when the parameter of interest is away from it.

2. THE REDUCED BASIS METHOD FOR VISCOUS FLOWS

In this section we formulate the reduced-basis method for viscous incompressible flows modeled by the Navier–Stokes equations. The Navier–Stokes equations, when written in primitive variables, are

$$\mathbf{u}_t - \nu\Delta\mathbf{u} + \mathbf{u}\cdot\nabla\mathbf{u} + \nabla p = \mathbf{f} \quad \text{in } \Omega \times (0, T], \tag{2.1}$$

$$\nabla\cdot\mathbf{u} = 0 \quad \text{in } \Omega \times (0, T], \tag{2.2}$$

$$\mathbf{u} = \mathbf{b} \quad \text{on } \Gamma \times [0, T], \tag{2.3}$$

$$\mathbf{u}(0, \mathbf{x}) = \mathbf{u}_0(\mathbf{x}) \quad \text{in } \Omega, \tag{2.4}$$

where $\mathbf{u}(t, \mathbf{x})$ and $p(t, \mathbf{x})$ denote the velocity and pressure, respectively, $\mathbf{f}(t, \mathbf{x})$ is the body force per unit mass, ν is the kinematic viscosity, and $\mathbf{u}_0$ is the initial velocity. Furthermore, T is a positive constant, $\mathbf{b}$ is the boundary velocity, and Ω is a bounded region in $\mathbb{R}^2$ whose boundary is Γ.

We choose a variational formulation and finite element method to approximate (2.1)–(2.4), but other methods can also be used with the reduced-basis method. Casting (2.1)–(2.4) in appropriate variational form requires the introduction of some notations.

2.1. *Notations*

We denote by $L^2(\Omega)$ the collection of square-integrable functions defined on Ω and we denote the associated norm by $\|\cdot\|_0$. Let

$$H^1(\Omega) = \left\{ v \in L^2(\Omega) : \frac{\partial v}{\partial x_i} \in L^2(\Omega) \text{ for } i = 1, 2 \right\},$$
$$H_0^1(\Omega) = \{ v \in H^1 : v|_{\partial\Omega} = 0 \},$$
$$L_0^2(\Omega) = \left\{ q \in L^2(\Omega) : \int_\Omega q \, d\Omega = 0 \right\}.$$

We define the standard bilinear and trilinear forms associated with the Navier–Stokes problem,

$$a(\mathbf{u}, \mathbf{v}) = \int_\Omega \nabla \mathbf{u} : \nabla \mathbf{v} \, d\Omega \quad \text{for all } \mathbf{u}, \mathbf{v} \in \mathbf{H}^1(\Omega);$$

here the colon notation stands for the scalar product on $\mathbb{R}^{2\times 2}$,

$$b(\mathbf{u}, q) = -\int_\Omega q \nabla \cdot \mathbf{u} \, d\Omega \quad \text{for all } \mathbf{u} \in \mathbf{H}^1(\Omega) \; \forall q \in L^2(\Omega)$$

and

$$c(\mathbf{u}, \mathbf{v}, \mathbf{w}) = \int_\Omega (\mathbf{u} \cdot \nabla)\mathbf{v} \cdot \mathbf{w} \, d\Omega \quad \text{for all } \mathbf{u}, \mathbf{v}, \mathbf{w} \in \mathbf{H}^1(\Omega).$$

For given $\mathbf{b} \in \mathbf{H}^{1/2}(\Gamma)$ and the boundary condition

$$\mathbf{u} = \mathbf{b} \text{ on } \Gamma \text{ with } \int_\Gamma \mathbf{b} \cdot \mathbf{n} \, d\Gamma = 0,$$

we define

$$\mathbf{V_b} = \{ \mathbf{u} \in \mathbf{H}^1(\Omega) : \mathbf{u} = \mathbf{b} \text{ on } \Gamma, \; \mathbf{b} \in \mathbf{H}^{1/2}(\Gamma) \}.$$

We now summarize some properties of these linear forms. We have the coercivity relations associated with $a(\cdot, \cdot)$,

$$a(\mathbf{u}, \mathbf{u}) = \|\nabla \mathbf{u}\|_0^2 \geq C_0 \|\mathbf{u}\|_1^2 \quad \text{for all } \mathbf{u} \in \mathbf{H}_0^1(\Omega)$$

which is a direct consequence of Poincaré inequality. The forms $a(\cdot, \cdot)$, $b(\cdot, \cdot)$, and $c(\cdot, \cdot, \cdot)$ are all continuous; in particular, we have

$$|c(\mathbf{u}, \mathbf{v}, \mathbf{w})| \leq C_1 \|\mathbf{u}\|_1 \|\mathbf{v}\|_1 \|\mathbf{w}\|_1.$$

The bilinear form $b(\cdot, \cdot)$ satisfies the following inf-sup condition:

$$\inf_{q \in L_0^2(\Omega)} \sup_{\mathbf{v} \in \mathbf{H}_0^1(\Omega)} \int_\Omega q \nabla \cdot \mathbf{v} \, d\Omega \geq C_2 \|q\| \, \|\mathbf{v}\|_1.$$

2.2. *Variational Formulation.*

We derive a variational formulation of the problem (2.1)–(2.4) by multiplying both sides of (2.1) and (2.2) by $\mathbf{v} \in \mathbf{H}_0^1(\Omega)$ and $q \in L^2(\Omega)$, respectively, and applying the divergence theorem. The variational problem becomes
Find $\mathbf{u} \in L^2(0, T; \mathbf{V_b})$ *and* $p \in L^2(0, T; L_0^2(\Omega))$ *such that*

$$(\mathbf{u}_t, \mathbf{v}) + \frac{1}{Re} a(\mathbf{u}, \mathbf{v}) + c(\mathbf{u}, \mathbf{u}, \mathbf{v}) + b(\mathbf{v}, p) = (\mathbf{f}, \mathbf{v}) \quad \textit{for all } \mathbf{v} \in \mathbf{H}_0^1(\Omega), \tag{2.5}$$

$$b(\mathbf{u}, q) = 0 \quad \textit{for all } q \in L_0^2(\Omega), \tag{2.6}$$

and

$$\mathbf{u}(0, \mathbf{x}) = \mathbf{u}_0(\mathbf{x}) \quad \textit{for } \mathbf{x} \in \Omega.$$

A typical finite element approximation of (2.5)–(2.6) is to seek solutions $\mathbf{u}^h(t, \cdot) \in \mathbf{V_b^h} \subset \mathbf{V_b}$ and $p^h(t, \cdot) \in S_0^h \subset L_0^2(\Omega)$,

$$\left(\mathbf{u}_t^h, \mathbf{v}^h\right) + \frac{1}{Re} a(\mathbf{u}^h, \mathbf{v}^h) + c(\mathbf{u}^h, \mathbf{u}^h, \mathbf{v}^h) + b(\mathbf{v}^h, p^h) = (\mathbf{f}, \mathbf{v}^h) \quad \text{for all } \mathbf{v}^h \in \mathbf{V}_0^h \tag{2.7}$$

and

$$b(\mathbf{u}^h, q^h) = 0 \quad \text{for all } q^h \in S_0^h, \tag{2.8}$$

where $\mathbf{V}_0^h \subset \mathbf{H}_0^1(\Omega)$ and $S_0^h \subset L_0^2(\Omega)$ are approximating finite element subspaces, and we are setting $Re = 1/\nu$ which is the Reynolds number; i.e., the variables are appropriately nondimensionalized. We will denote the solution of the finite-dimensional equations (2.7)–(2.8) at a fixed time t_i by $\mathbf{u}^h(t_i, \cdot)$ and $p^h(t_i, \cdot)$. Further details regarding the notations and formulation given in the last two sections can be found in [17].

2.3. *The Reduced-Basis Method and Reduced-Order Model*

In this section, we will present the reduced-basis method and the reduced-order model for viscous flows.

2.3.1. *Case I: Steady state.* Let us illustrate the derivation of a reduced-order model using the Lagrange basis elements using the formalism and terminology used in [15, 5]. Let the Lagrange basis elements $\{\boldsymbol{\phi}_i\}$ be given by $\boldsymbol{\phi}_i = \mathbf{u}^h$. One can generate such basis elements by solving

$$\frac{1}{Re} a(\mathbf{u}^h, \mathbf{v}^h) + c(\mathbf{u}^h, \mathbf{u}^h, \mathbf{v}^h) + b(\mathbf{v}^h, p^h) = (\mathbf{f}, \mathbf{v}^h) \quad \text{for all } \mathbf{v}^h \in \mathbf{V}_0^h \tag{2.9}$$

and

$$b(\mathbf{u}^h, q^h) = 0 \quad \text{for all } q^h \in S_0^h \tag{2.10}$$

for different values of parameter μ, where $\mu = Re$. Thus, given a set of values for the Reynolds number $\{\mu_i : i = 1, 2, 3, ...M\}$, we solve (2.9)–(2.10) M times to determine the

set $\{\hat{\mathbf{u}}_m : m = 1, \ldots, M\}$, where $\hat{\mathbf{u}}_i = \mathbf{u}^h(\mu_i)$. We then set

$$\mathbf{V}^M = \text{span}\{\hat{\mathbf{u}}_i : i = 1, ..., M\} \subset \mathbf{V}^h.$$

We next briefly describe the *Hermite approach* in this setting. Let $\mathbf{u}_i = \mathbf{u}(\mu_i) \in \mathbf{V}^h$ and $\mathbf{u}_i' = (\partial \mathbf{u}^h/\partial\mu)(\mu_i) \in \mathbf{V}_0^h$; then solve

$$\frac{1}{\mu_i} a(\mathbf{u}_i', \mathbf{v}^h) + c(\mathbf{u}_i', \mathbf{u}_0, \mathbf{v}^h) + c(\mathbf{u}_0, \mathbf{u}_i', \mathbf{v}^h) + b(\mathbf{v}^h, p_i') = \frac{1}{\mu_i^2} a(\mathbf{u}_i, \mathbf{v}^h) \quad \text{for all } \mathbf{v}^h \in \mathbf{V}_0^h$$

and

$$b(\mathbf{u}_i', q^h) = 0 \quad \text{for all } q^h \in S_0^h$$

to obtain $\mathbf{u}_i'$. We then set

$$V^M = \text{span}\{\mathbf{u}_i, \mathbf{u}_i' : i = 1, \ldots, M\}.$$

Once we have a set of reduced basis functions we write the *reduced-order model* in the form: seek $\mathbf{u}^M \in \mathbf{V}^M \subset \mathbf{V}^h$ such that

$$\frac{1}{Re} a(\mathbf{u}^M, \mathbf{v}^M) + c(\mathbf{u}^M, \mathbf{u}^M, \mathbf{v}^M) = (\mathbf{f}, \mathbf{v}^M) \quad \text{for all } \mathbf{v}^M \in \mathbf{V}_0^M, \tag{2.11}$$

where $\mathbf{V}_0^m = \mathbf{V}^m \cap \mathbf{V}_0^h$. Note that, by construction $\mathbf{u}^M$ automatically satisfies (2.10) and, due to the global support of the reduced-basis elements, the system (2.11) is equivalent to a dense lower order nonlinear system of equations as opposed to the system (2.9)–(2.10) which is a sparse nonlinear system due to the local support of the basis. Our computational experiments and the other computations reported in the references mentioned earlier seem to indicate that an accurate approximation can be obtained for a large range of parameter values using 5 to 10 basis elements. Therefore, although the resulting reduced-order model is dense, it is small compared to the sparse but large systems that result from the standard basis functions.

2.3.2. *Case II: Time-dependent state.* Let us illustrate the derivation of a reduced-order model using the Lagrange basis elements. Let the Lagrange basis elements $\{\boldsymbol{\phi}_i\}$ be given by $\boldsymbol{\phi}_i = \mathbf{u}^h(t_i, \cdot)$. We can generate such basis elements by using the implicit Euler method with appropriate step size to integrate (2.7) in time, and then we select the discrete time solution $\{\hat{\mathbf{u}}_i\}$ at a given set of values $\{t_i\}$, $i = 1, \ldots, M$. We then obtain $\mathbf{V}^R = \text{span}\{\hat{\mathbf{u}}_i : i = 1, \ldots, M\}$. Due to the nonhomogeneous boundary condition, we have that the reduced-basis subspace $\mathbf{V}^R$ consists of the trial and test functions, where the test functions in $\mathbf{V}_0^R = \mathbf{V}^R \cap \mathbf{V}_0^h$ satisfy the homogeneous boundary condition. Once we have a set of reduced-basis functions we write the *reduced-order model* in the form: seek $\mathbf{u}^M(t, \cdot) \in \mathbf{V}^M = \text{span}\{\mathbf{u}_i : i = 1, \ldots, M\} \subset \mathbf{V}^h$ such that

$$\left(\mathbf{u}_t^M, \mathbf{v}^M\right) + \frac{1}{Re}(\nabla \mathbf{u}^M, \nabla \mathbf{v}^M) + (\mathbf{u}^M \cdot \nabla \mathbf{u}^M, \mathbf{v}^M) = (\mathbf{f}, \mathbf{v}^M) \quad \text{for all } \mathbf{v}^M \in \mathbf{V}_0^M, \tag{2.12}$$

$$(\mathbf{u}^M, \mathbf{v}^M)_\Gamma = (\mathbf{u}_b, \mathbf{v}^M)_\Gamma \quad \text{for all } \mathbf{v}^M \in \mathbf{V}^M|_\Gamma, \tag{2.13}$$

and

$$(\mathbf{u}(0,\mathbf{x}),\mathbf{v}^M)=(\mathbf{u}_0(\mathbf{x}),\mathbf{v}^M)\quad\text{for all}\,\mathbf{v}^M\in\mathbf{V}_0^M,\tag{2.14}$$

where $\mathbf{V}_0^M=\mathbf{V}^M\cap\mathbf{V}_0^h$.

3. COMPUTATIONS OF THE REDUCED ORDER MODEL

In this section we will test the performance of reduced-order model (2.11) in two well-known test problems in fluid flows, namely driven cavity flow and backward-facing-step channel flow. We will demonstrate via these tests that the reduced-basis method can be used, not only in the interpolary mode, but also in the extrapolary mode with very few basis elements. Let us first consider the stationary case.

3.1. *Stationary Driven Cavity Problem*

The problem we are about to describe is a classical driven cavity flow. Various researchers have studied this problem computationally using a variety of methods and formulations. We can think of this as a fluid-filled cavity bounded by rigid walls at $x=0$, $x=1$, $y=0$, and a top wall that is moving with unit speed. We consider, of course, a two-dimensional situation. The domain is divided into rectangles and we further divide each rectangle into triangles. Then we choose quadratic polynomials defined on these triangles to approximate velocity fields, and for the approximation of pressure we choose linear polynomials defined on the same triangles.

In all our computations reported in this article, we define the Reynolds number as $Re=V\cdot L/\nu$. In the driven cavity problem, $V=$ top surface velocity, $L=$ cavity dimension, $\nu=$ kinematic viscosity of the fluid. We assume throughout the simulations that $V=1$, $L=1$, and hence $Re=1/\nu$.

The computation using the reduced-basis method is done by first selecting basis elements and then defining test functions and trial functions such that they are linearly independent and the test functions satisfy homogeneous boundary conditions. We generate basis elements $\{\mathbf{u}_i\}_{i=1}^M\subset\mathbf{V}^M$ for the reduced-order model by computing the solutions at M different Reynolds numbers to the full steady state Navier–Stokes equations,

$$\frac{1}{Re}a(\mathbf{u}^h,\mathbf{v}^h)+c(\mathbf{u}^h,\mathbf{u}^h,\mathbf{v}^h)+b(\mathbf{v}^h,p^h)=(\mathbf{f},\mathbf{v}^h)\quad\text{for all}\,\mathbf{v}^h\in\mathbf{V}_0^h,\tag{3.1}$$

$$b(\mathbf{u}^h,q^h)=0\quad\text{for all}\,q^h\in S_0^h,\tag{3.2}$$

and $\mathbf{u}=(1,0)$ on the top boundary and everywhere else on the boundary no slip boundary conditions are assumed.

Given the basis elements $\{\mathbf{u}\}_{i=1}^M$, the reduced-order solution $\mathbf{u}^h$ is formed by setting

$$\mathbf{u}^M=\sum_{i=1}^M\alpha_i\boldsymbol{\phi}_i,\tag{3.3}$$

where $\boldsymbol{\phi}_i=\mathbf{u}_{i+1}-\mathbf{u}_i$, $i=1,2,\ldots,M-1$, and $\boldsymbol{\phi}_M=\mathbf{u}_M$. We further take $\alpha_M=1$ so that

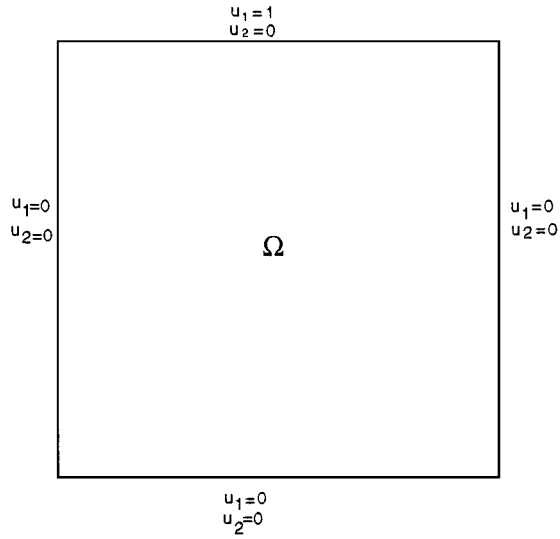

FIG. 1. Schematic of driven cavity.

the boundary conditions are satisfied. The solution $\mathbf{u}^M$ is computed from

$$\frac{1}{Re}a(\mathbf{u}^M, \mathbf{v}^M) + c(\mathbf{u}^M, \mathbf{u}^M, \mathbf{v}^M) = (\mathbf{f}, \mathbf{v}^M) \quad \text{for all } \mathbf{v}^M \in \mathbf{V}_0^M, \tag{3.4}$$

where $\mathbf{V}_0^M = \text{span}\{\boldsymbol{\phi}_i : i = 1, \ldots, M-1\}$ is the span of the test functions.

Let us rewrite (3.4) using the representation (3.3) with $\alpha_i \in \mathbb{R}$. Using (3.3) and taking $\mathbf{v}^M = \boldsymbol{\phi}_j$, $j = 1, \ldots, M-1$, in (3.4), we get for $j = 1, ..., M-1$

$$\frac{1}{Re}\sum_{i=1}^{M-1}\alpha_i(\nabla\boldsymbol{\phi}_i, \nabla\boldsymbol{\phi}_j) + \left(\sum_{i=1}^{M-1}\alpha_i\boldsymbol{\phi}_i \cdot \nabla\sum_{k=1}^{M-1}\alpha_k\boldsymbol{\phi}_k, \boldsymbol{\phi}_j\right) = (\mathbf{f}, \boldsymbol{\phi}_j),$$

or equivalently, the following nonlinear algebraic equations

$$\mathcal{A}\boldsymbol{\alpha} + \boldsymbol{\alpha}^t\mathcal{N}\boldsymbol{\alpha} = F, \tag{3.5}$$

where the stiffness matrix $\mathcal{A} = (\mathcal{A}_{ij})$, the forcing term $F = (F_i)$ and $\boldsymbol{\alpha} = (\alpha_i)$,

$$\mathcal{A}_{ij} = \frac{1}{Re}(\nabla\boldsymbol{\phi}_i, \nabla\boldsymbol{\phi}_j),$$
$$F_i = (F, \boldsymbol{\phi}_i).$$

Moreover, the quadratic form $\boldsymbol{\alpha}^t\mathcal{N}\boldsymbol{\alpha}$ corresponds to the trilinear form in (2.5) restricted to the reduced basis space $\mathbf{V}^R$ and is given by $(\boldsymbol{\alpha}^t\mathcal{N}\boldsymbol{\alpha})_i = \boldsymbol{\alpha}^t\mathcal{P}_i\boldsymbol{\alpha}$, where $\mathcal{P}_i \in \mathbb{R}^{M\times M}$ is defined by

$$(\mathcal{P}_i)_{kl} = (\boldsymbol{\phi}_k \cdot \nabla\boldsymbol{\phi}_l, \boldsymbol{\phi}_i).$$

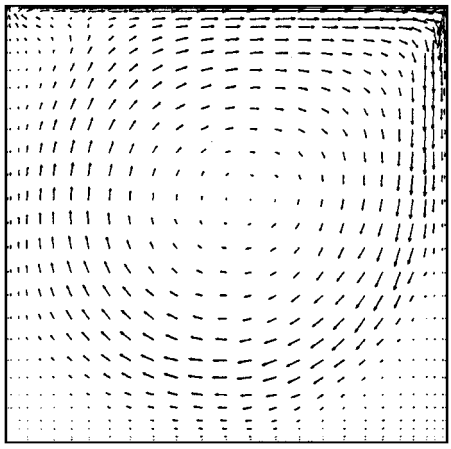

FIG. 2. Reduced solution with 4 basis: $Re = 1200$.

We choose the basis elements for the reduced-order model (3.5) by computing the lid-driven cavity flow at Reynolds numbers, 100, 300, 500, 700, and 900. The computations are done with a 29×29 nonuniform mesh. Our goal here is to show one can use the reduced-basis method in an extrapolary mode and still get reasonable results. We choose the Reynolds numbers to be 1200 and 1500 and compare the reduced-order model solution with the solution to the full model at those Reynolds numbers.

The nonlinear algebraic equations (3.5) were solved using the Newton's iterative method. The computed solutions of the driven cavity flow at $Re = 1200$ using the reduced-order model and the full model are in good agreement, (see Figs. 2–3). We also studied the effects of the number of basis elements used in the reduced-order model. The l_2-norm difference between the reduced and full solution is given in Tables 1–2 and a comparison of u-velocity along the vertical centerline of the cavity is given in Figs. 4–5. They all indicate that the reduced-basis method can, in fact, give very good results, even in the extrapolary

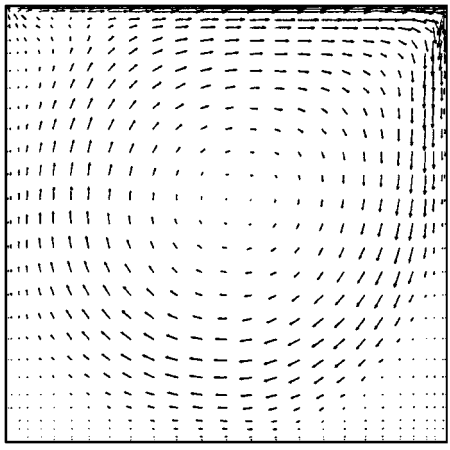

FIG. 3. Solution to full system: $Re = 1200$.

TABLE 1
l_2 Difference of Solutions at $Re = 1200$

Basis elements	2	3	4	5
$\|\mathbf{u}_r - \mathbf{u}_f\|_2$	.3989	.06913	.0600	.04322

mode and with few elements. Similar results have been reported in [15] using the Taylor approach.

Finally, we turn to a comparison study of the Lagrange approach versus the Hermite approach. The basis elements for the Lagrange approach were selected at Reynolds numbers 100, 300, 500, and 700, and for the Hermite approach they were selected at 300 and 700. The comparison was carried out by computing the driven cavity flow at Reynolds number 1200. For the Hermite approach the test function selection is $\boldsymbol{\phi}_1 = \mathbf{u}_{700} - \mathbf{u}_{300}$, $\boldsymbol{\phi}_2 = 300\mathbf{u}'|_{300}$, and $\boldsymbol{\phi}_3 = 700\mathbf{u}'|_{700}$. The solution is then sought as

$$\mathbf{u} = \mathbf{u}_{700} + \sum_{i=1}^{3} \alpha_i \boldsymbol{\phi}_i$$

and then the nonlinear algebraic equations (3.5) were solved using the Newton iterative method.

Figure 6 shows the u-velocity at the vertical centerline of the cavity using the Hermite and Lagrange approaches. The l_2-norm difference between the full solution and the reduced-basis solution using these two approaches are $|\mathbf{u}_l - \mathbf{u}_f|_2 = 0.0889$ and $|\mathbf{u}_h - \mathbf{u}_f|_2 = 0.0766$, where $\mathbf{u}_l$ is the solution obtained using the Lagrange approach and $\mathbf{u}_h$ is that obtained using the Hermite approach. According to our comparison with the driven cavity problem, the performance of the Hermite approach is better than that of Lagrange.

3.2. *Unsteady Channel Problem*

We demonstrate the feasibility of the reduced-basis method in unsteady problems by studying the channel flow past a backward-facing step. This problem has been extensively studied both experimentally and computationally. A schematic of the geometry is given in Fig. 13. The height of the inflow boundary is 0.5 and that of the outflow boundary is 1. The length of the narrower section of the channel is 1 and that of wider section of the channel is 7 (the total horizontal length is 8). We choose the viscosity constant $\nu = 1/1000$. At the inflow we assume the flow is parabolic and we take $\mathbf{u}(y) = \mathbf{u}_i = 8(y - 0.5)(1 - y)$. At the outflow boundary, we again assume the flow is parabolic and $\mathbf{u} = \mathbf{u}_o = y(1 - y)$. The prescribed body force $\mathbf{f}$ is chosen to be zero.

Triangular finite elements are chosen to discretize the domain. This choice is natural since we use a nonuniform mesh with local refinements around the corner of the step and

TABLE 2
l_2 Difference between Solutions at $Re = 1500$

Basis elements	2	3	4	5
$\|\mathbf{u}_r - \mathbf{u}_f\|_2$	.5504	.0729	.0698	.0545

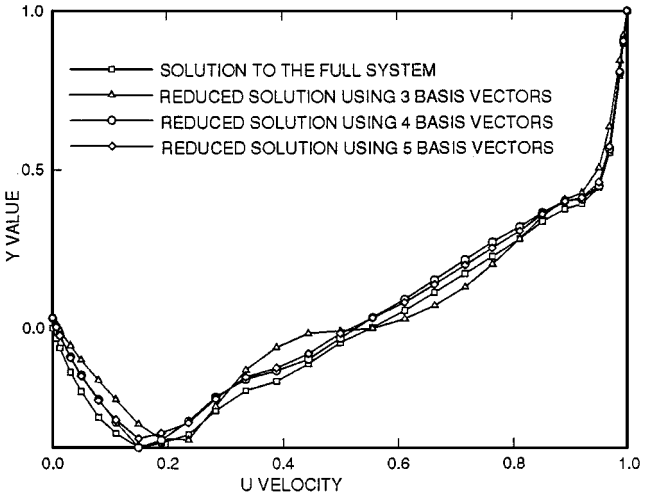

FIG. 4. Comparison of reduced basis solution to full solution at $Re = 1200$.

near the top of the no-slip wall. The velocity and pressure are approximated by piecewise quadratic and piecewise linear polynomials, respectively.

We generate basis elements $\{\mathbf{u}_i\}_{i=1}^{M} \subset \mathbf{V}^M$ for the reduced-order model by computing the solutions at M different times for the full unsteady Navier–Stokes equations:

$$\left(\frac{\partial}{\partial t}\mathbf{u}^h, \mathbf{v}^h\right) + \frac{1}{Re}a(\mathbf{u}^h, \mathbf{v}^h) + c(\mathbf{u}^h, \mathbf{u}^h, \mathbf{v}^h) + b(\mathbf{v}^h, p^h) = (\mathbf{f}, \mathbf{v}^h) \quad \text{for all } \mathbf{v}^h \in \mathbf{V}_0^h \tag{3.6}$$

$$b(\mathbf{u}^h, q^h) = 0 \quad \text{for all } q^h \in S_0^h, \tag{3.7}$$

and we assume fully developed flow at the inflow and outflow boundary. Everywhere else on the boundary the no-slip boundary condition is assumed.

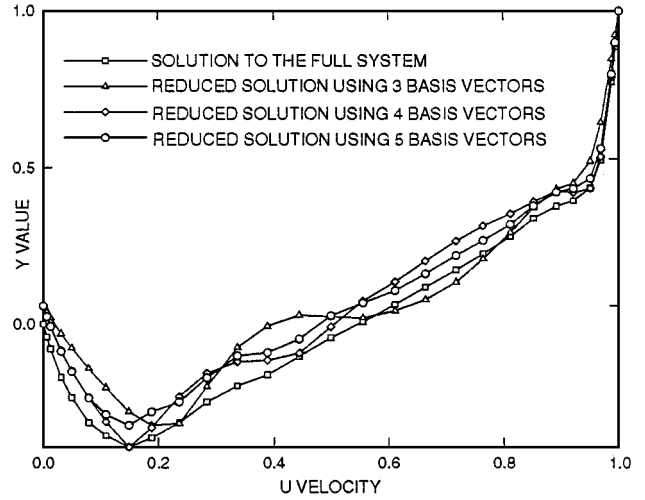

FIG. 5. Comparison of reduced basis solution to full solution at $Re = 1500$.

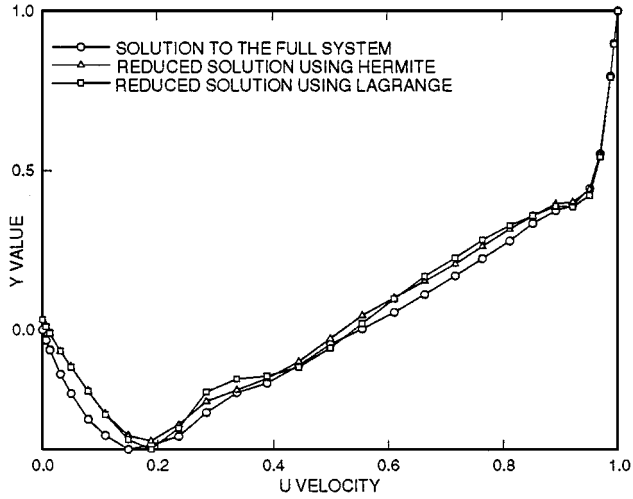

FIG. 6. Comparison of Hemite solution to Lagrange solution with 4 basis elements at $Re = 1200$.

Given the basis elements $\{\mathbf{u}_i\}_{i=1}^M$, the reduced-order solution $\mathbf{u}^M$ is formed by setting

$$\mathbf{u}^M(t) = \sum_{i=1}^{M} \alpha_i(t)\boldsymbol{\phi}_i, \tag{3.8}$$

where $\boldsymbol{\phi}_i = \mathbf{u}_{i+1} - \mathbf{u}_i$, $i = 1, 2, \ldots, M-1$, and $\boldsymbol{\phi}_M = \mathbf{u}_M$. We further take $\alpha_M = 1$ so that the boundary conditions are satisfied. The solution $\mathbf{u}^M$ is computed from

$$\left(\frac{\partial}{\partial t}\mathbf{u}^M, \mathbf{v}^M\right) + \frac{1}{Re}a(\mathbf{u}^M, \mathbf{v}^M) + c(\mathbf{u}^M, \mathbf{u}^M, \mathbf{v}^M) = (\mathbf{f}, \mathbf{v}^M) \quad \text{for all } \mathbf{v}^M \in \mathbf{V}_0^M, \tag{3.9}$$

where $\mathbf{V}_0^M = \text{span}\{\boldsymbol{\phi}_i : i = 1, \ldots, M-1\}$ is the span of the test functions.

Let us rewrite (3.9) using the representation (3.8) with $\alpha_i(t) \in \mathbb{R}$. Using (3.8) and taking $\mathbf{v}^R = \boldsymbol{\phi}_j$, $j = 1, \ldots, M-1$, in (3.9), we get for $j = 1, \ldots, M-1$ and $t \in I$

$$\sum_{i=1}^{M-1}\dot{\alpha}_i(t)(\boldsymbol{\phi}_i, \boldsymbol{\phi}_j) + \frac{1}{Re}\sum_{i=1}^{M-1}\alpha_i(t)(\nabla\boldsymbol{\phi}_i, \nabla\boldsymbol{\phi}_j) + \left(\sum_{i=1}^{M-1}\alpha_i(t)\boldsymbol{\phi}_i \cdot \nabla\sum_{k=1}^{M-1}\alpha_k(t)\boldsymbol{\phi}_k, \boldsymbol{\phi}_j\right)$$

$$= (\mathbf{f}, \boldsymbol{\phi}_j), \quad \sum_{i=1}^{M-1}\alpha_i(0)(\boldsymbol{\phi}_i, \boldsymbol{\phi}_j) = (\mathbf{u}_0, \boldsymbol{\phi}_j),$$

or equivalently, the nonlinear ordinary differential equations

$$\begin{aligned} \mathcal{M}\dot{\boldsymbol{\alpha}}(t) + \mathcal{A}\boldsymbol{\alpha}(t) + \boldsymbol{\alpha}^t\mathcal{N}\boldsymbol{\alpha} &= F(t), \\ \mathcal{M}\boldsymbol{\alpha}(0) &= U^0, \end{aligned} \tag{3.10}$$

where the mass matrix $\mathcal{M} = (\mathcal{M}_{ij})$, the stiffness matrix $\mathcal{A} = (\mathcal{A}_{ij})$, the forcing term $F = (F_i)$,

FIG. 7. Full solution when $t = 10$ and $Re = 1000$.

$\boldsymbol{\alpha} = (\alpha_i)$, and the initial condition $U^0 = (U_i^0)$:

$$\begin{aligned} \mathcal{M}_{ij} &= (\boldsymbol{\phi}_i, \boldsymbol{\phi}_j), \\ \mathcal{A}_{ij} &= \frac{1}{Re}(\nabla\boldsymbol{\phi}_i, \nabla\boldsymbol{\phi}_j), \\ F_i(t) &= (F(t), \boldsymbol{\phi}_i), \\ U_i^0 &= (\mathbf{u}_0, \boldsymbol{\phi}_i). \end{aligned}$$

We selected $\{t_i\}$ at 11 time instances between 1 and 11 for the basis element generation in the construction of (3.10). Then the initial value problem for the nonlinear ODE (3.10) was solved using the implicit Euler method for the time discretization with the time step 10^{-3} and the Newton iterative method. The computational domain was divided into triangles with a refined grid near the flow separation. Our computational experiments on the backward facing step channel flow and on unsteady cavity flow (not reported here) indicate the clear and promising ability of the reduced-order model in predicting the dynamics of fluid flows. Figures 7–8 are the channel flow computations with the full model and the reduced-order model at time $t = 10$, respectively.

4. CONTROL OF REDUCED ORDER MODEL

In this section, we will formulate some optimal control problems in fluid flows using boundary surface movement as the control mechanism. We define reduced-order control problems using the reduced-basis method and the reduced-order models developed in the previous sections. The resulting reduced-order control problems are then solved via the necessary conditions of optimality by applying Newton's method.

In order to develop the framework for the application of the reduced-basis method for the control of fluid flows, let us first formulate an optimal control problem:

$$\text{Minimize } \mathcal{J}(\mathbf{u}, g) \tag{4.1}$$

subject to

$$-\frac{1}{Re}\Delta\mathbf{u} + \mathbf{u}\cdot\nabla\mathbf{u} + \nabla p = \mathbf{f} \quad \text{in } \Omega, \tag{4.2}$$

$$\nabla\cdot\mathbf{u} = 0 \quad \text{in } \Omega, \tag{4.3}$$

$$\mathbf{u}|_{\Gamma_1} = \mathbf{b}, \tag{4.4}$$

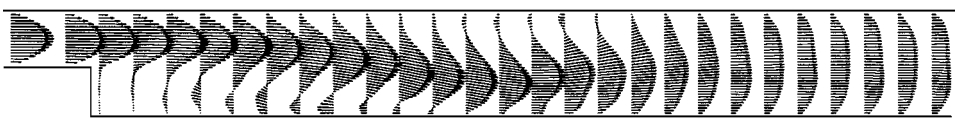

FIG. 8. Reduced basis solution when $t = 10$ and $Re = 1000$.

and

$$\mathbf{u}|_{\Gamma_2} = g\boldsymbol{\tau}. \tag{4.5}$$

We discuss the boundary control problem and, thus, the body force $\mathbf{f}$ is fixed. The function g is the control input that influences the flow through the movement of part of the boundary Γ_2, the function $\mathbf{b}$ is a fixed boundary value on Γ_1, and $\boldsymbol{\tau}$ is a unit tangential vector. We note here that this control mechanism is nondestructive in the sense that no mass is added to the system.

A variational form of (4.2)–(4.5) is defined in the unsteady setting as:

Find $\mathbf{u} \in \mathbf{V_b}$ *and* $p \in L_0^2(\Omega)$ *such that*

$$\frac{1}{Re}a(\mathbf{u}, \mathbf{v}) + c(\mathbf{u}, \mathbf{u}, \mathbf{v}) + b(\mathbf{v}, p) = (\mathbf{f}, \mathbf{v}) \quad \textit{for all } \mathbf{v} \in \mathbf{H}_0^1(\Omega) \tag{4.6}$$

and

$$b(\mathbf{u}, q) = 0 \quad \textit{for all } q \in L_0^2(\Omega). \tag{4.7}$$

We will study two control problems that are cast in the framework of (4.1)–(4.5):

($\mathcal{C}_1$) The cavity control problem with the cost function

$$\mathcal{J}(\mathbf{u}) = \int_\Omega |\mathbf{u} - \mathbf{u}_d|^2 \, d\Omega.$$

($\mathcal{C}_2$) The channel control problem with the cost function

$$\mathcal{J}(\mathbf{u}) = \int_\Omega |\nabla \times \mathbf{u}|^2 \, d\Omega.$$

Regarding the set of admissible controls g, we assume that the set $\mathcal{U}$ of admissible controls g is closed and bounded in $\mathbb{R}$.

Defining the set

$$S = \{\mathbf{u} \in \mathbf{H}^1(\Omega) : g \in \mathcal{U}, \ \mathbf{u} \text{ satisfies (4.2)–(4.5)}\},$$

we have the following theorem regarding the existence of optimal control (see, e.g. [3, 4, 6, 7, 16] for a detailed discussions on this topic).

THEOREM 4.1. *Suppose* $\mathcal{U}$ *is compact. Then* S *is bounded in* $\mathbf{H}^1(\Omega)$ *and the control problems* ($\mathcal{C}_1$) *and* ($\mathcal{C}_2$) *have solutions.*

Proof. An outline of the proof follows. First we define appropriate extensions $\mathbf{u}_1$ and $\mathbf{u}_2$ to the boundary values (4.4) and (4.5), respectively, and redefine (4.2)–(4.5) with a change of variable $\mathbf{u} = \mathbf{v} + g\mathbf{u}_1 + \mathbf{u}_2$ such that the velocity $\mathbf{v}$ now satisfies homogeneous boundary values. The next step is to estimate the terms in the variational form of (4.2)–(4.5) using the coercivity and continuity properties of the bilinear and trilinear forms and the antisymmetry property of the trilinear form.

The second assertion follows from the observation that the cost functionals are weakly sequentially lower semicontinuous and bounded below by zero, the solution set S is bounded in a Hilbert space $\mathbf{H}^1(\Omega)$, the set $\mathcal{U}$ is compact, and $\mathbf{H}^1(\Omega)$ is compactly embedded in $\mathbf{L}^4(\Omega)$. Then, if we take a minimizing sequence $(\mathbf{u}_n, g_n) \in S \times \mathcal{U}$, there is a limit $(\mathbf{u}^*, g^*)$ to this sequence and the limit is in fact a minimum to the control problem. ∎

To solve the control problems, we will use constrained minimization techniques based on the necessary condition of optimality. Let us first derive the necessary conditions of optimality for our control problems. To facilitate the forthcoming discussion we cast the control problems in the abstract setting: *For* $(\mathbf{u}, g) \in \mathbf{H}_0^1(\Omega) \times \mathcal{U}$

$$\begin{aligned} &\textit{Minimize} \quad \mathcal{J}(\mathbf{u}, g) \\ &\textit{subject to} \quad \mathcal{G}(\mathbf{u}, p, g) = 0 \textit{ and } \mathcal{H}(\mathbf{u}) = 0, \end{aligned}$$

where $\mathcal{G}(\mathbf{u}, p, g) = 0$ now represents the Navier–Stokes constraint (4.6) and $\mathcal{H}(\mathbf{u} = 0)$ is the divergence-free condition (4.7). Then the Lagrangian can be written as

$$\mathcal{L}(\mathbf{v}, p, g, \lambda, \sigma) = \mathcal{J}(\mathbf{u}, g) + < \boldsymbol{\lambda}, \mathcal{G}(\mathbf{u}, p, g) > + < \sigma, \mathcal{H}(\mathbf{u}) >,$$

where $\mathbf{u} = \mathbf{v} + g\mathbf{u}_1 + \mathbf{u}_2$ and $\boldsymbol{\lambda}$ and σ are Lagrange multipliers. The existence of Lagrange multipliers is guaranteed by the regular point condition; i.e., the linearized constraint is surjective. Before discussing the regular point condition further, let us define the variational form of the gradient of the constraints. Given $(\boldsymbol{\chi}, q, h) \in \mathbf{H}_0^1(\Omega) \times L_0^2(\Omega) \times \mathbb{R}$,

$$\begin{aligned} < \boldsymbol{\Psi}, \mathcal{G}'(\mathbf{u}, g)(\boldsymbol{\chi}, q, h) > + < r, \mathcal{H}'(\mathbf{u})(\boldsymbol{\chi}) > = &\frac{1}{Re} a(\boldsymbol{\chi} + h\mathbf{u}_1, \boldsymbol{\Psi}) + c(\boldsymbol{\chi} + h\mathbf{u}_1, \mathbf{u}, \boldsymbol{\Psi}) \\ &+ c(\mathbf{u}, \boldsymbol{\chi} + h\mathbf{u}_1, \boldsymbol{\Psi}) + b(q, \boldsymbol{\Psi}) \\ &+ b(\boldsymbol{\chi} + h\mathbf{u}_1, r) \end{aligned}$$

for all $(\boldsymbol{\Psi}, r) \in \mathbf{H}_0^1(\Omega) \times L_0^2(\Omega)$. We then have the following equivalent solvability condition for the regular point condition:

Setting $\boldsymbol{\Phi} = \boldsymbol{\chi} + h\mathbf{u}_1$ the solvability condition can be written as: given $\mathbf{s} \in \mathbf{H}^{-1}(\Omega)$ find $\boldsymbol{\Phi} \in \mathbf{H}^1(\Omega)$ and $r \in L_0^2(\Omega)$ such that

$$\frac{1}{\mathrm{Re}} a(\boldsymbol{\Phi}, \boldsymbol{\Psi}) + c(\boldsymbol{\Phi}, \mathbf{u}, \boldsymbol{\Psi}) + c(\mathbf{u}, \boldsymbol{\Phi}, \boldsymbol{\Psi}) + b(\boldsymbol{\Psi}, r) = < \mathbf{s}, \boldsymbol{\Psi} > \quad \text{for all } \boldsymbol{\Psi} \in \mathbf{H}_0^1(\Omega)$$

and

$$b(\boldsymbol{\Phi}, q) = 0 \quad \text{for all } q \in L_0^2(\Omega).$$

The solvability of this system can be shown at least when the data are small. Next as a result of the regular point condition [10], we have

THEOREM 4.2. *Suppose the regular point condition is satisfied. Then we obtain the first-order necessary condition for* $(\mathbf{v}, p, g, \boldsymbol{\lambda}, \sigma) \in \mathbf{H}_0^1(\Omega) \times L_0^2(\Omega) \times \mathbb{R} \times \mathbf{H}_0^1(\Omega) \times L_0^2(\Omega)$

$$\begin{aligned} \frac{\partial \mathcal{L}}{\partial \mathbf{v}}(\boldsymbol{\chi}) = &\frac{1}{Re} a(\boldsymbol{\lambda}, \boldsymbol{\chi}) + c(\boldsymbol{\chi}, \mathbf{u}, \boldsymbol{\lambda}) + c(\mathbf{u}, \boldsymbol{\chi}, \boldsymbol{\lambda}) + b(\boldsymbol{\chi}, \sigma) \\ &+ < \mathcal{J}'(\mathbf{u}), \boldsymbol{\chi} > = 0 \quad \textit{for all } \boldsymbol{\chi} \in \mathbf{H}_0^1(\Omega), \end{aligned} \tag{4.8}$$

$$\frac{\partial \mathcal{L}}{\partial g} = a(\mathbf{u}_1, \boldsymbol{\lambda}) + c(\mathbf{u}, \mathbf{u}_1, \boldsymbol{\lambda}) + c(\mathbf{u}_1, \mathbf{u}, \boldsymbol{\lambda}) + b(\mathbf{u}_1, \sigma) + < \mathcal{J}'(\mathbf{u}), \mathbf{u}_1 > = 0, \tag{4.9}$$

and

$$\frac{\partial \mathcal{L}}{\partial p}(q) = b(\boldsymbol{\lambda}, q) = 0 \quad \textit{for all } q \in L_0^2(\Omega). \tag{4.10}$$

The system (4.6)–(4.10) characterizes the optimal control and optimal states and we call this the optimality system.

4.1. *Reduced-Order Control Problem*

Using the notations and the framework introduced in Section 3, we can cast the control problems $(\mathcal{C}_1)$ and $(\mathcal{C}_2)$ in the general *reduced-order control formulation*

$$\text{Minimize } \mathcal{J}(x) = \left(\frac{1}{2} x^t \mathcal{Q} x - x \cdot \mathbf{d} + c\right)$$

subject to

$$\mathcal{A} x + x^t \mathcal{N} x = 0,$$

where $x = (\alpha, u)^T$ is the state. Moreover, for the control problem $(\mathcal{C}_1)$

$$\mathcal{Q}_{i,j} = (\boldsymbol{\phi}_i, \boldsymbol{\phi}_j), \quad \mathbf{d}_i = (\mathbf{u}_d, \boldsymbol{\phi}_i), \quad c = \frac{1}{2}|\mathbf{u}_d|^2$$

and for the control problem $(\mathcal{C}_2)$

$$\mathcal{Q}_{i,j} = (\nabla \times \boldsymbol{\phi}_i, \nabla \times \boldsymbol{\phi}_j), \quad \mathbf{d}_i = c = 0.$$

Following the derivation of the optimality system given for the optimal control problem (4.1)–(4.5), one can derive an optimality system for the above reduced-order control problem (P^R). In the numerical simulations we report in the sequel we solve the optimality system corresponding to the reduced-order control problem (P^R) by applying Newton's method.

4.2. *Control of Driven Cavity Flow*

In this section we formulate and numerically solve a control problem in a driven cavity using the reduced-basis method. The problem is that of finding the bottom surface velocity g such that the fluid velocity $\mathbf{u}$ is driven to a desired state $\mathbf{u}_d$. This control problem can be cast as a minimization problem with the cost function

$$\mathcal{J}(\mathbf{u}) = \int_\Omega |\mathbf{u} - \mathbf{u}_d|^2 \, d\Omega$$

and subject to the constraint that the fluid obeys the equation of motion, where $\mathbf{u}_d$ is the desired velocity field.

The geometry of the problem and the finite element approximations have already been discussed in Section 3.1. Replacing the cost function in $(\mathcal{C}_1)$ in the abstract problem, the control problem for the driven cavity is written as

$$\text{Minimize } \mathcal{J}(\mathbf{u}) = \int_\Omega |\mathbf{u} - \mathbf{u}_d|^2 \, d\Omega \tag{4.11}$$

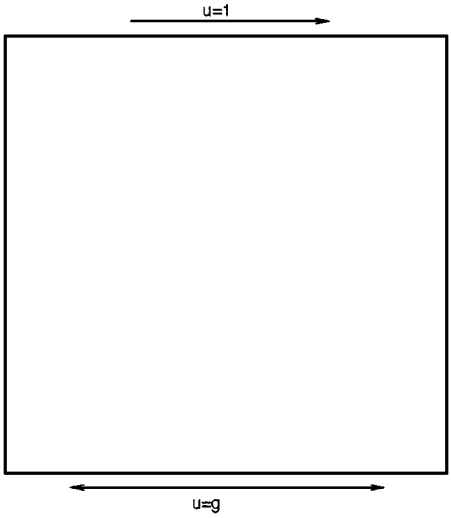

FIG. 9. Schematic of controlled driven cavity.

subject to

$$\frac{1}{Re}a(\mathbf{u},\mathbf{v})+c(\mathbf{u},\mathbf{u},\mathbf{v})+b(\mathbf{v},p)=(\mathbf{f},\mathbf{v})\quad\text{for all}\,\mathbf{v}\in\mathbf{H}_0^1(\Omega) \tag{4.12}$$

and

$$b(\mathbf{u},q)=0\quad\text{for all}\,q\in L_0^2(\Omega), \tag{4.13}$$

$$\mathbf{u}\,|_{\Gamma_{\text{top}}}=(U^{\text{top}},0),\quad \mathbf{u}\,|_{\Gamma_{\text{bot}}}=(g,0),\quad \mathbf{u}\,|_{\Gamma_{\text{side}}}=(0,0),$$

where U^{top}, g are top and bottom surface velocities, respectively. We wish to find the control input g such that the flow matches as close as possible the desired flow $\mathbf{u}_d$. The top velocity is fixed throughout the problem. Figure 9 gives the physical domain and the boundary conditions.

Using the reduced-basis method, the control problem (4.11)–(4.13) is first approximated by a reduced-order control problem of the form (P^R). In order to achieve this, basis elements are computed with the boundary conditions described in Table 3. The test functions $\{\boldsymbol{\phi}_1,\boldsymbol{\phi}_2\}$ are chosen so that they have zero boundary conditions. The trial function $\boldsymbol{\phi}_3=\mathbf{u}_4$ corresponds to the control force satisfying $\boldsymbol{\phi}_3|_{\Gamma_{\text{bot}}}\neq 0$ and it satisfies the zero boundary conditions everywhere else. Then we seek the solution as

$$\mathbf{u}^M=\mathbf{u}_1+g\mathbf{u}_4+\sum_{i=1}^{2}\alpha_i\boldsymbol{\phi}_i,$$

TABLE 3
Wall Velocities for Basis Vector Generation

Basis elements	$\mathbf{u}_1$	$\mathbf{u}_2$	$\mathbf{u}_3$	$\mathbf{u}_4$
Top wall velocity	1	1	1	0
Bottom wall velocity	0	1	−1	1

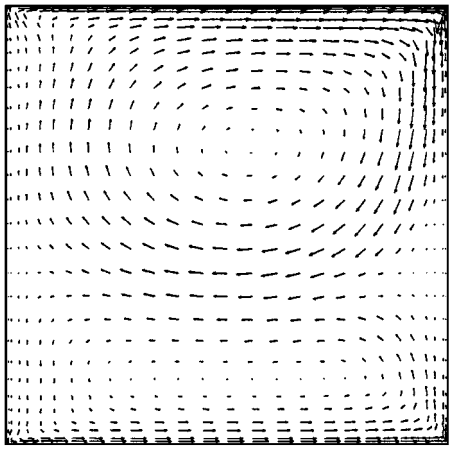

FIG. 10. Desired velocity field at $Re = 500$.

where g is the control (tangential velocity at the boundary), $\boldsymbol{\phi}_1 = \mathbf{u}_2 - \mathbf{u}_1 - \mathbf{u}_4$, and $\boldsymbol{\phi}_2 = \mathbf{u}_3 - \mathbf{u}_1 + \mathbf{u}_4$. We take $\mathbf{V}_0^M = \text{span}\{\boldsymbol{\phi}_1, \boldsymbol{\phi}_2\}$.

The computation of the optimal control for the reduced-order control problem is carried out in two steps: First the necessary conditions of the optimality system (4.6)–(4.10) are derived for the reduced-order control problem. Then this system is solved by applying Newton's method. As a consequence, the calculated control in general provides a *suboptimal control* to the original control problem (4.11)–(4.13). The computations for this problem were done with 29×29 nonuniform mesh and the Reynolds number was 500 ($\nu = 1/500$). The top wall velocity is taken to be $U^{\text{top}} = 1$ and the desired velocity $\mathbf{u}_d$ is computed with the bottom wall moving at one-half of the top wall velocity. We get control $g^{\text{opt}} = 0.4806$ in four Newton iterations and the corresponding boundary velocity therefore is 0.4806. The resulting flow field is given in Fig. 11. We also carried out computations to find the flow field corresponding to the optimal control input computed from the reduced-order model which is given in Fig. 12. They all are in good agreement with the desired flow field given in Fig. 10.

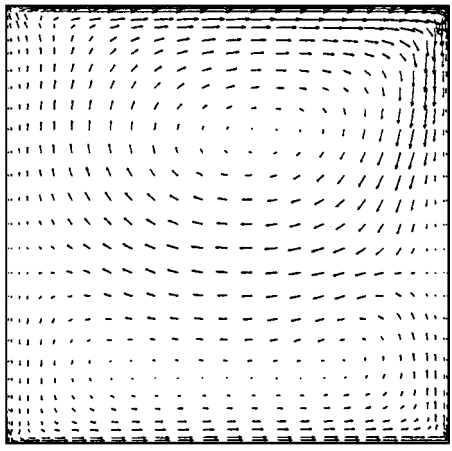

FIG. 11. Controlled velocity field at $Re = 500$.

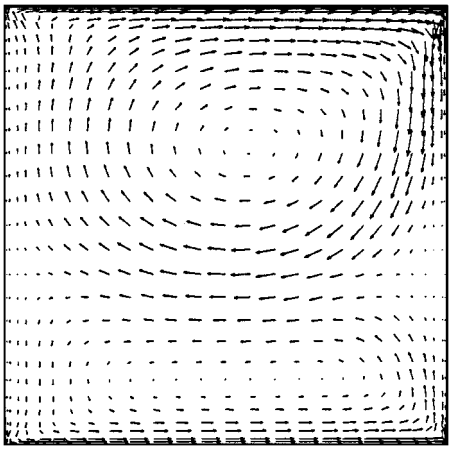

FIG. 12. Cavity flow with optimal control input at $Re = 500$.

4.3. *Control of Channel Flows*

In this section, we consider the problem of control of the channel flows. We will consider two different geometrical configurations, namely the forward-facing step and the backward-facing step. Schematics of these geometries are given in Fig. 13 and Fig. 17. The aim is to shape the flow to a desired configuration by means of controlled movement of the boundary along some part of the boundary. In this work we consider the minimization of vorticity in the flow. Thus, we consider the cost functional

$$\mathcal{J}(\mathbf{u}) = \int_\Omega |\nabla \times \mathbf{u}|^2 \, d\Omega,$$

where $\boldsymbol{\omega} = \nabla \times \mathbf{u}$ is the vorticity. The control problem for the channel is posed in the form

$$\text{Minimize } \mathcal{J}(\mathbf{u}) = \int_\Omega |\nabla \times \mathbf{u}|^2 \, d\Omega \tag{4.14}$$

subject to

$$\frac{1}{Re} a(\mathbf{u}, \mathbf{v}) + c(\mathbf{u}, \mathbf{u}, \mathbf{v}) + b(\mathbf{v}, p) = (\mathbf{f}, \mathbf{v}) \quad \text{for all } \mathbf{v} \in \mathbf{H}_0^1(\Omega), \tag{4.15}$$

$$b(\mathbf{u}, q) = 0 \quad \text{for all } q \in L_0^2(\Omega), \tag{4.16}$$

$$\mathbf{u}|_{\Gamma_1} = \mathbf{b}, \quad \text{and} \quad \mathbf{u}|_{\Gamma_2} = g\boldsymbol{\tau},$$

where Γ_2 is part of the boundary where the boundary surface is moving (control input) and Γ_2 is the rest of the boundary. Then $\mathbf{b} \in \mathbf{H}^{1/2}(\Gamma)$ corresponds to the inflow, outflow

FIG. 13. Schematic of controlled backward-facing-step channel.

boundary conditions and zero boundary conditions at the walls. Also, g is the magnitude of the boundary surface velocity. In the following we will consider two channel geometries and in each of them our choice of control portion Γ_2 is not the only one possible. Our particular choice is motivated by the fact that if one wants maximum influence in the flow, then the control has to be applied in that vicinity.

4.3.1. *Case I: Backward-facing-step channel flow.* First we consider a control problem in a backward-facing-step channel flow. We assume that the inflow and outflow are parabolic as elaborated in Section 3.2. Figure 15 qualitatively demonstrates the situation for a high Reynolds number. As mentioned previously, the aim is to shape the flow to a desired configuration by controlled boundary movement. A desirable flow, of course, depends on the situation in which the flow occurs. Here our objective is to remove the recirculation that occurs in the corner region. Thus, the control portion Γ_2 is taken to be the line segment between $y = 0$ and $y = 0.5$ at $x = 1$, where we note that at $x = 1$ is where the channel changes its cross section area. Also, we take $\boldsymbol{\tau} = (1, 0)$; that is, the movement of the wall is vertical and thus $g \in \mathbb{R}$ completely determines the control input.

Using the reduced-basis method, the control problem (4.14)–(4.16) is first approximated by a reduced-order control problem of the form (P^R). In order to achieve this, basis elements are computed with the boundary conditions described in Table 4. The test functions $\{\boldsymbol{\phi}_1, \ldots, \boldsymbol{\phi}_4\}$ are chosen so that they have zero boundary conditions. The trial function $\boldsymbol{\phi}_5$ corresponds to the control force such that $\boldsymbol{\phi}_5|_{\Gamma_1} = 0$ and $\boldsymbol{\phi}_5|_{\Gamma_2} \neq 0$. Then we set

$$\mathbf{u} = \mathbf{u}_1 + g\boldsymbol{\phi}_5 + \sum_{i=1}^{4} \alpha_i \boldsymbol{\phi}_i,$$

where $\boldsymbol{\phi}_1 = \mathbf{u}_3 - 2\mathbf{u}_2 + \mathbf{u}_1$, $\boldsymbol{\phi}_2 = \mathbf{u}_4 - 3\mathbf{u}_2 + 2\mathbf{u}_1$, $\boldsymbol{\phi}_3 = \mathbf{u}_5 - 4\mathbf{u}_2 + 3\mathbf{u}_1$, $\boldsymbol{\phi}_4 = \mathbf{u}_6 - 5\mathbf{u}_2 + 4\mathbf{u}_1$, and $\boldsymbol{\phi}_5 = \mathbf{u}_6 - \mathbf{u}_1$. The reduced-order control problem was solved by applying Newton's method to the corresponding optimality system. Then, for the vorticity cost functional $(\mathcal{C}_2)$, with the Reynolds number 200 ($\nu = 1/200$), we obtain the optimal control $g^{\text{opt}} = 0.2601$ in five Newton iterations and the corresponding optimal boundary velocity therefore is -0.13005. The resulting flow is shown in Fig. 14. We also simulated the flow corresponding to the optimal control computed from the reduced-order model and the result is shown in Fig. 16. The results show significant reduction in the corner circulation.

4.3.2. *Case II: Forward-facing-step channel flow.* The second case we investigate is the control of forward-facing-step channel flow. We assume that the inflow and outflow are parabolic with $u(y) = u_i = y(1-y/3)/3$ and $u(y) = u_o = 3(3-y)(y-1)/8$, respectively. Figure 18 qualitatively demonstrates the situation for a high Reynolds number. Out objective in this case is to remove the recirculation that occurs on the top of the step.

Using the reduced-basis method, the control problem (4.14)–(4.16) is first approximated by a reduced-order control problem of the form (P^R). In order to achieve this, basis elements are computed with the boundary conditions described in Table 5. The test functions

TABLE 4
Wall Velocities for Basis Vector Generation

Basis elements	$\mathbf{u}_1$	$\mathbf{u}_2$	$\mathbf{u}_3$	$\mathbf{u}_4$	$\mathbf{u}_5$	$\mathbf{U}_6$
Wall velocity	0	-0.1	-0.2	-0.3	-0.4	-0.5

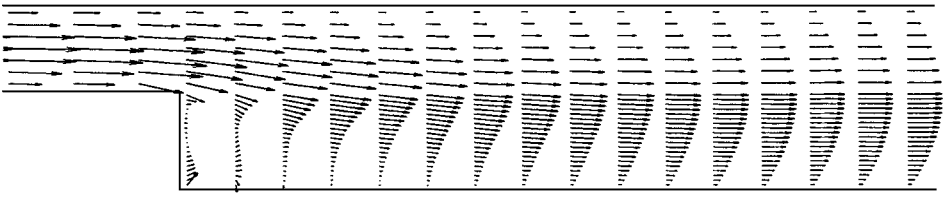

FIG. 14. Controlled velocity field at $Re = 200$.

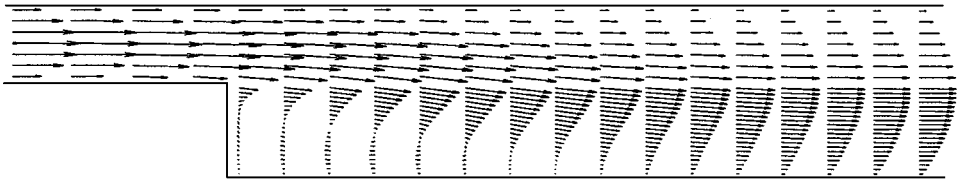

FIG. 15. Uncontrolled velocity field at $Re = 200$.

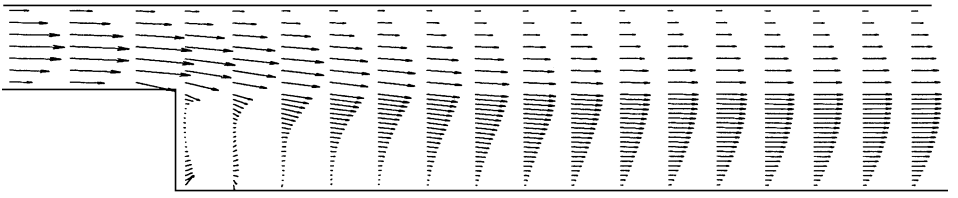

FIG. 16. Channel flow with optimal control input at $Re = 200$.

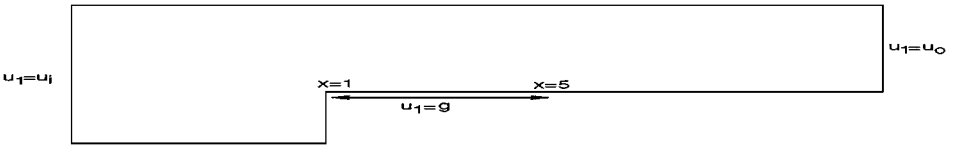

FIG. 17. Schematic of controlled forward-facing-step channel.

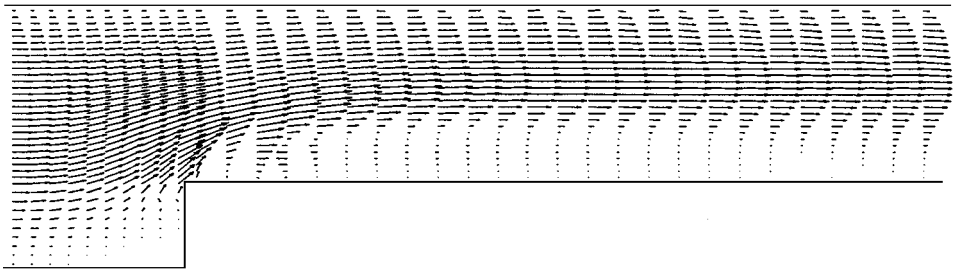

FIG. 18. Uncontrolled velocity field at $Re = 1000$.

TABLE 5
Wall Velocities for Basis Vector Generation

Basis elements	$\mathbf{u}_1$	$\mathbf{u}_2$	$\mathbf{u}_3$	$\mathbf{u}_4$	$\mathbf{u}_5$	$\mathbf{u}_6$
Wall velocity	0	0.1	0.15	0.2	0.25	0.3

$\{\boldsymbol{\phi}_1, \ldots, \boldsymbol{\phi}_4\}$ are chosen so that they have zero boundary conditions. The trial function $\boldsymbol{\phi}_5$ corresponds to the control force such that $\boldsymbol{\phi}_5|_{\Gamma_1} = 0$ and $\boldsymbol{\phi}_5|_{\Gamma_2} \neq 0$. Then we set

$$\mathbf{u} = \mathbf{u}_1 + g\boldsymbol{\phi}_5 + \sum_{i=1}^{4} \alpha_i \boldsymbol{\phi}_i,$$

where $\boldsymbol{\phi}_1 = \mathbf{u}_6 - 3\mathbf{u}_2 + 2\mathbf{u}_1$, $\boldsymbol{\phi}_2 = \mathbf{u}_6 - 2\mathbf{u}_3 + \mathbf{u}_1$, $\boldsymbol{\phi}_3 = \mathbf{u}_6 - 1.5\mathbf{u}_4 + 0.5\mathbf{u}_1$, $\boldsymbol{\phi}_4 = \mathbf{u}_6 - 1.2\mathbf{u}_5 + 0.2\mathbf{u}_1$, and $\boldsymbol{\phi}_5 = \mathbf{u}_6 - \mathbf{u}_1$.

We take the control region to be the line segment between $x = 1$ and $x = 5$ at $y = 3$. Here we note that at $y = 3$ is where the channel changes its cross section area. Also, we take $\boldsymbol{\tau} = (1, 0)$, that is, the movement of the wall is horizontal and, like in the previous case, $g \in \mathbb{R}$ completely determines the control input.

Then, for the vorticity cost ($\mathcal{C}_2$), with the Reynolds number 1000 ($\nu = 1/1000$), we obtain the optimal control $g^{\text{opt}} = 0.3041$ in 17 Newton iterations and the corresponding optimal boundary velocity therefore is 0.09120. The resulting flow is shown in Fig. 19. We also simulated the flow corresponding to the optimal control computed from the reduced-order model and the result is shown in Fig. 20. The results show significant reduction in the corner circulation.

5. CONCLUSION

In this article we have presented a reduced-order modeling approach for simulation and control of viscous incompressible flows. The reduced-order models suitable for control and which capture the essential physics were developed using the reduced-basis method. Numerical simulations performed on the reduced-order model demonstrated that it can be used, not only in the interpolary, but also in the extrapolary mode. Feasibility of the reduced-order method for flow control was demonstrated on two boundary control problems using boundary surface movement as a control mechanism. Through our computational

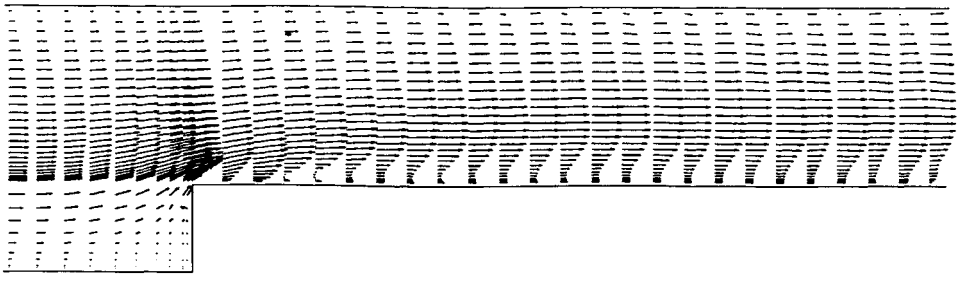

FIG. 19. Controlled channel flow at $Re = 1000$.

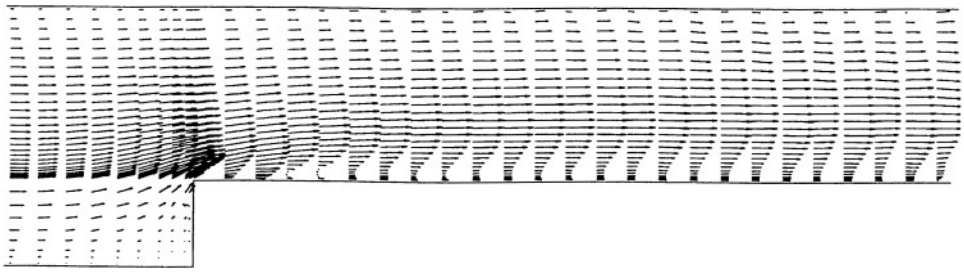

FIG. 20. Channel flow with optimal control input at $Re = 1000$.

experiments we have demonstrated the feasibility and applicability of the reduced-order method for simulation and control of fluid flows.

REFERENCES

1. B. O. Almroth, P. Stern, and F. A. Brogan, Automatic choice of global shape functions in structural analysis, *AIAA J.* **16**, 525 (1978).
2. J. A. Burns and Y.-R. Ou, Feedback control of the driven cavity problem using LQR designs, in *Proc. 33rd IEEE Conference on Decision and Control, Florida, 1994*, p. 289.
3. M. Desai and K. Ito, Optimal controls of Navier–Stokes equations, *SIAM J. Control Optim.* **32**, 1428 (1994).
4. H. O. Fattorini and S. S. Sritharan, Existence of optimal controls for viscous flow problems, *Proc. R. Soc. London Ser. A* **439**, 81 (1992).
5. M. D. Gunzburger, *Finite Element Methods for Viscous Incompressible Flows* (Academic Press, London, 1989).
6. M. D. Gunzburger, L. S. Hou, and T. P. Svobodny, Boundary velocity control of incompressible flow with an application to viscous drag reduction, *SIAM J. Control Optim.* **30**, 167 (1992).
7. L. S. Hou and S. S. Ravindran, A penalized Neumann control approach for solving an optimal Dirichlet control problem for the Navier–Stokes equations, *SIAM J. Control Optim.* to appear.
8. L. S. Hou and S. S. Ravindran, Computations of boundary optimal control problems for an electrically conducting fluid, *J. Comput. Phys.* **128**(2), 319 (1996).
9. K. Ito and S. S. Ravindran, Reduced basis method for flow control, in *Proceedings of the 35th Conference on Decision and Control, IEEE, Kobe, Japan, 1996*, p. 3705.
10. H. Mauer and J. Zowe, First and second order necessary and sufficient optimality conditions for infinite-dimensional programming problems, *Math Programming* **16**, 98 (1979).
11. D. Nagy, Modal representation of geometrically nonlinear behavior by the finite element method, *Comput. & Struct.* **10**, 683 (1979).
12. A. K. Noor, Recent advances in reduction methods for nonlinear problems, *Comput. & Struct.* **13**, 31 (1981).
13. A. K. Noor, C. M. Anderson, and J. M. Peters, Reduced basis technique for collapse analysis of shells, *AIAA J.* **19**, 393 (1981).
14. A. K. Noor and J. M. Peters, Tracking post-limit-paths with reduced basis technique, *Comput. Methods Appl. Mech. Eng.* **28**, 217 (1981).
15. J. S. Peterson, The reduced basis method for incompressible viscous flow calculations, *SIAM J. Sci. Stat. Comput.* **10**, 777 (1989).
16. S. S. Sritharan, Dynamic programming of Navier–Stokes equations, *System & Control Lett.* **16**, 299 (1991).
17. R. Temam, *Navier–Stokes Equations: Theory and Numerical Analysis* (North-Holland, Amsterdam, 1986).